

# Magnetic Studies of End-Chain Spin Effects in the Haldane Gap Material $\text{Ni}(\text{C}_3\text{H}_{10}\text{N}_2)_2\text{N}_3(\text{ClO}_4)$

G. E. Granroth\*, S. Maegawa†, and M. W. Meisel

Department of Physics, University of Florida, P.O. Box 118440, Gainesville, FL 32611-8440.

J. Krzystek and L.-C. Brunel

Center for Interdisciplinary Magnetic Resonance, National High Magnetic Field Laboratory, 1800 East Paul Dirac Drive, Tallahassee, FL 32306-4005.

N. S. Bell and J. H. Adair

Department of Materials Science and Engineering, University of Florida, P.O. Box 116400, Gainesville, FL 32611-6400.

B. H. Ward, G. E. Fanucci, L.-K. Chou‡, and D. R. Talham

Department of Chemistry, University of Florida, P.O. Box 117200, Gainesville, FL, 32611-7200.

(May 19, 2018)

Electron spin resonance (ESR), at 9, 94, and 190 GHz, and magnetization studies on polycrystalline, powder, and ultrafine powder samples of  $\text{Ni}(\text{C}_3\text{H}_{10}\text{N}_2)_2\text{N}_3(\text{ClO}_4)$  (NINAZ) have revealed several effects arising from the Haldane phase. Using the  $g$  value of the end-chain spin  $S$  as determined by ESR, our results confirm that the end-chain spins are  $S = \frac{1}{2}$  and show no evidence for  $S = 1$  end-chains. In addition, the ESR signals reveal spectral weight consistent with a model describing interactions between the end-chain spins on the shortest chains and between the magnetic excitations on the chains and the end-chain spins.

76.30.-v, 75.10.Jm, 75.50 -y

Since Haldane's suggestion [1] of an energy gap in the excitation spectrum for integer spin Heisenberg antiferromagnetic chains, significant progress has been made in experimentally and theoretically understanding these systems. The Haldane gap has been observed in a myriad of  $S = 1$  materials [2–9], and one  $S = 2$  system [10]. Theoretically, the valence bond solid model [11] provides a physically intuitive picture of  $S = 1$  antiferromagnetic chains, and one prediction is that the chains should terminate with end-chain spins of  $S = \frac{1}{2}$ . The presence of these end-chains was identified initially by electron spin resonance (ESR) in samples of  $\text{Ni}(\text{C}_2\text{H}_8\text{N}_2)_2\text{NO}_2(\text{ClO}_4)$  (NENP) doped with both magnetic [12] and non-magnetic impurities [13]. However, this identification was challenged by Ramirez *et al.* [14] who performed specific heat measurements on pure and doped samples of  $\text{Y}_2\text{BaNiO}_5$ . These results were interpreted to suggest that, for chains up to  $\sim 250$  spins long, the end-chains were  $S = 1$  entities existing in either a singlet or triplet ground state, depending on whether the chain consisted of an even or odd number of spins. An even/odd chain length effect is not expected for chains longer than  $\sim 50$  spins [15,16], and the data of Ramirez *et al.* [14] have been described by  $S = \frac{1}{2}$  end-chains experiencing a strong anisotropy [17,18]. Although subsequent experiments [19–21] have been interpreted in terms of  $S = \frac{1}{2}$  end-chains, these studies have not conclusively eliminated the  $S = 1$  possibility. The Haldane gap material  $\text{Ni}(\text{C}_3\text{H}_{10}\text{N}_2)_2\text{N}_3(\text{ClO}_4)$  (NINAZ) [3] is well-suited for the study of end-chain spins. Our magnetization and

ESR results are completely consistent with only the presence of  $S = \frac{1}{2}$  end-chains. Furthermore, Mitra, Halperin, and Affleck (MHA) [22] have described the temperature dependence of the ESR intensity originating from the  $S = \frac{1}{2}$  end-chains, and they have made predictions about the contributions to the linewidth arising from interactions between the end-chain spins on the shortest chains and between the magnetic excitations on the chains and the end-chain spins. Although the temperature dependence of the central peak of the ESR signal in *doped* samples of NENP [12,22] and TMNIN [20] has been described by the MHA picture, experimental evidence for the interactions has not been reported. Once again, due to its properties, *undoped* NINAZ is ideally suited to observe this phenomenon, and this Letter provides the first experimental evidence of these fundamental interactions.

In many instances, non-magnetic dopants are used to increase the end-chain spin concentration [13,14,17,19–21,23,24], but unfortunately, doped samples have their limitations. For example in NENP doped beyond  $\sim 0.5\%$ , the dopant no longer breaks chains by direct substitution [25]. Even in materials with a non-magnetic isomorph (*e.g.*  $\text{Ni}(\text{C}_4\text{H}_6\text{N}_2)_2(\text{C}_2\text{O}_4)$  [19]), doping beyond a certain level is nonlinear with respect to the number of observed end-chain spins. Furthermore, dopants cause changes in the magnetic environment and may shift, split, and/or broaden the ESR spectra. NINAZ [3] circumvents doping difficulties because it shatters while passing through a structural phase transition at  $\sim 255$  K [26], thereby producing end-chain spins with-

out doping [3,26,27]. In other words, the intrinsic and uncontrolled shattering processes afford the distinct advantage of avoiding the complications associated with using dopants.

Two batches of NINAZ were prepared according to the procedure of Gadet *et al.* [26] as modified by Chou [28]. The room temperature crystal structure [28] was found to be consistent with the one proposed by Gadet *et al.* [26], exhibiting a  $Ni - Ni$  distance of  $a = 5.849 \text{ \AA}$ . The magnetic properties of NINAZ have been measured by several groups [3,6,26,27], and neutron scattering measurements [9] have provided a direct measurement of the intrachain exchange energy  $J = 125 \text{ K}$ , the Haldane gap  $\Delta = 41.9 \text{ K}$ , the single-ion anisotropy  $D = 21 \text{ K}$ , and the spin wave velocity  $c = 2.55 \times 10^4 \text{ m/s}$ . A magnetic field,  $H$ , greater than 30 T is required to close the Haldane gap [6], and consequently, the application of 5 T at 2 K will not appreciably affect the Haldane state. Since the nascent crystals shattered upon cooling but remained oriented, these specimens are referred to as *polycrystalline* samples. To increase the number of end-chain spins, two techniques were used to grind the samples. Initial grindings used a pestle and mortar to produce a sample referred to as *powder*. Subsequent grindings, using a standard ball mill, produced a sample referred to as *ultrafine powder*. Centrifugal sedimentation was used to characterize the grain size for powder and ultrafine powder samples (inset of Fig. 1). In addition, inductively coupled plasma mass spectrometry indicated that the level of extrinsic magnetic impurities was no greater than a few parts per billion for any of the three sample types. Magnetization,  $M$ , as a function of  $H$  up to 5 T at  $T = 2 \text{ K}$  was measured using a commercial SQUID magnetometer. Our use of the  $M(H, 2 \text{ K})$  data ensures that the Haldane state is fully developed instead of being thermally smeared as it is in a full analysis of our  $\chi(2 \text{ K} \leq T \leq 300 \text{ K})$  results [29]. X-band ESR was performed with a commercial system tuned to a resonance frequency  $\nu = 9.25 \text{ GHz}$  and operating down to  $T = 4 \text{ K}$ . High frequency (93.93 and 189.87 GHz) ESR was performed at  $T = 5 \text{ K}$  in magnetic fields up to 14 T.

Figure 2 shows the  $M(H, 2 \text{ K})$  data for polycrystalline, powder, and ultrafine powder samples. The solid lines are fits using

$$M(H, T) = N_A g \mu_B [(1/2) N_{1/2} B_{1/2}(g \mu_B H / k_B T) + N_1 B_1(g \mu_B H / k_B T)], \quad (1)$$

where  $B_{1/2}(g \mu_B H / k_B T)$  and  $B_1(g \mu_B H / k_B T)$  are the Brillouin functions, and  $N_{1/2}$  and  $N_1$  are the concentrations of  $S = \frac{1}{2}$  and  $S = 1$  spins. For the fits,  $g = 2.174$  was determined from ESR measurements, leaving  $N_{1/2}$  and  $N_1$  as the only free parameters since no measurable amounts of other spin values are reasonably expected or were observed by any ESR frequency. The results of the fits are given in Table I and demonstrate that the end-

chain spins are predominately  $S = \frac{1}{2}$  and that only trace amounts of  $S = 1$ , consistent with the presence of some uncoupled  $Ni^{2+}$ , exist in any of the samples. If there were contributions from singlet and triplet ground states, one would expect significantly more  $S = 1$  than  $S = \frac{1}{2}$  spins. Furthermore, our high frequency ESR studies did not reveal any  $S = 1$  resonances. Consequently, we conclude all the end-chain spins are  $S = \frac{1}{2}$ .

For our 9.25 GHz ESR work, the measured derivative spectra were integrated at a variety of temperatures. In the MHA description [22], the temperature dependence of the intensity of the central peak is given by the fraction of finite-length chains in their ground state and may be written as

$$I(T) = I(0) \tanh \left( \frac{h\nu}{2k_B T} \right) \times \frac{\exp \left[ -(\pi^{-1/2} L_{min} \lambda_T^{-1} - 1) e^{\frac{-\Delta}{k_B T}} \right]}{1 + \pi^{-1/2} L_0 \lambda_T^{-1} e^{\frac{-\Delta}{k_B T}}}, \quad (2)$$

where  $\nu = 9.25 \text{ GHz}$ ,  $\lambda_T = \hbar c(2k_B T \Delta)^{-1/2}$ ,  $L_0$  is the average chain length, and  $L_{min}$  is the minimum chain length. Since the Haldane gap  $\Delta \approx 42 \text{ K}$  is independently known,  $L_0$  and  $L_{min}$  are the only parameters, and  $L_{min}$  is constrained by the strength of the interaction between the  $S = \frac{1}{2}$  spins on the shortest chains [22]. Figure 1 shows the temperature dependence of the intensity for the powder and ultrafine powder specimens and the results of fits using Eq. 2 with  $L_{min} = 60 \pm 20$  sites. Excellent agreement exists between the data and the fits when  $L_0 = 1590 \pm 50$  sites ( $\sim 0.9 \mu\text{m}$ ) for the powder and  $910 \pm 50$  sites ( $\sim 0.5 \mu\text{m}$ ) for the ultrafine powder. Comparison with the particle size analysis (inset of Fig. 1) confirms that the pestle and mortar grinding process only slightly reduces the average chain length when compared to the polycrystalline material [27], whereas ball milling produces chains of a length consistent with the particle size. Finally, the values of  $L_0$  may be compared to the ones obtained from the magnetization results. Assuming a Poisson distribution, the results listed in Table I suggest  $L_0 \approx 2300$  sites for the powder and  $\approx 1100$  sites for the ultrafine powder. Within reasonable expectations for the model and analysis, these values are consistent with the aforementioned ones.

In Fig. 3, typical 9.25 GHz ESR lines at  $T = 4 \text{ K}$  are plotted, showing that the full width at half maxima ( $FWHM$ ) for the polycrystalline, powder, and ultrafine powder samples are  $\approx 8 \text{ mT}$ ,  $\approx 7 \text{ mT}$ , and  $\approx 10 \text{ mT}$ , respectively. The temperature dependencies of the linewidths are shown in Fig. 3a. For  $T \leq 7 \text{ K}$ , the  $FWHM$  is temperature independent, and this limit is governed by the interactions between the  $S = \frac{1}{2}$  end-chains on the shortest chains. Following MHA [22], this interaction may be roughly estimated as

$$\epsilon = \Delta \exp(-L_{min}/\xi), \quad (3)$$

where  $\xi$  is the correlation length. When  $\Delta \approx 42$  K,  $\xi \approx 6$  [15,16], and  $L_{min} = 50$ , then the resultant energy is  $\epsilon \approx 10$  mK  $\approx 8$  mT [30].

When magnetic excitations are present on the chains, there are two mechanisms [22] by which these bosons may influence the linewidth. Firstly, bosons changing energy levels (via interactions with the end-chain spins) could affect the linewidth, where this change in energy is quantized in units of

$$\delta E \approx \frac{(\hbar\pi c)^2}{2\Delta L^2}. \quad (4)$$

Using the values quoted earlier and taking  $L = L_0$ ,  $\delta E \approx 5$  mT for the powder and  $\approx 12$  mT for the ultra-fine powder. These values of  $\delta E$  are about the size of the  $FWHM$ , and consequently, these interactions contribute to the linewidth once a chain acquires a boson. The temperature dependence of the linewidth near the central peak has been derived by MHA [22], so the  $FWHM$  may be modeled by

$$FWHM = \epsilon + \Lambda T \exp(-\Delta/k_B T), \quad (5)$$

where  $\Lambda$  is a parameter which is beyond the scope of the present MHA model. The temperature dependence of the  $FWHM$  is reasonably reproduced when  $\epsilon = 8$  mT and  $\Lambda = 35$  mT/K, as shown in Fig. 3a. In other words, the major contribution to the  $FWHM$ , at  $T \leq 7$  K, comes from the end-chain spins on the shortest chains interacting with each other and, at  $T \geq 7$  K, arises from the interactions between the magnetic excitations and the end-chain spins. Finally, the other possible broadening mechanism arises from a small change in the energy of a boson that experiences a phase shift when interacting with an end-chain spin. This effect is significantly weaker than the exchange of energy  $\delta E$  and, consequently, is not detectable in the present measurements.

Another effect shown in Fig. 3 is the multiple ESR peaks of the polycrystalline sample. The polycrystalline line is the superposition of two strong peaks, the main one at  $307.3 \pm 0.2$  mT and the other at  $318.4 \pm 0.4$  mT. While the 307 mT line is due to the  $S = \frac{1}{2}$  end-chains, the intensity of the 318 mT peak depends both on the number of times the sample is cycled through the structural transition as well as the crystal used, suggesting that this peak is a consequence of the shattering process [29]. Since  $S = 1$  spins and extrinsic impurities are not possible explanations, one may consider changes in the magnetic environment due to chemical differences at surface sites or a dipolar interaction with a nearby end-chain spin. These possibilities may be examined by rotating the sample, but the lines observed with our undoped materials were rotationally invariant. On the other hand, in addition to the main ESR line which did not move when the sample was rotated, 0.5% Hg doped polycrystalline specimens exhibited lines which were dependent on orientation (see Fig. 3b). These results indicate different

magnetic sites were within our resolution and illustrate a reason why linewidth measurements of other systems failed to detect the presence of interactions (*i.e.* doping broadens the main line and adds other extrinsic ones).

In conclusion, our studies of the end-chains of NINAZ have experimentally confirmed fundamental theoretical predictions about quantum spin chains. Firstly, our magnetization and ESR measurements identify the presence of  $S = \frac{1}{2}$  end-chains (see Figs. 1 - 3) and detect no evidence of  $S = 1$  end-chain spins. Secondly, our ESR studies reveal spectral weight arising from the interaction between the end-chain spins on the shortest chains and between the magnetic excitations on the chains and the end-chain spins.

We thank W. W. Kim, P. J. C. Signore, M. Escobar, and R. Russell for contributions to this work. We have enjoyed communications or discussions with J. H. Barry, T. M. Brill, E. Dagotto, A. Feher, K. Hallberg, A. K. Hassan, J. K. Ingersent, Th. Jolicœur, K. Majumdar, S. E. Nagler, M. Orendáč, C. Saylor, F. Sharifi, and A. Sikkema. This work was supported, in part, by funding from the NSF through DMR-9200671 (M.W.M.), DMR-9530453 (D.R.T.), and the NHMFL.

\*Present address: Oak Ridge National Laboratory, P.O. Box 2008, MS-6393, Oak Ridge, TN 37831-6393.

†Present and permanent address: Graduate School of Human and Environmental Studies, Kyoto University, Kyoto 606-01, Japan.

‡Present address: Winbond Electronics Corp, No. 4 Creatioin Rd. III, Science-based Industrial Park, Hsinchu, Taiwan, R.O.C.

---

- [1] F. D. M. Haldane, Phys. Rev. Lett. **50**, 1152 (1983).
- [2] J. P. Renard *et al.*, Europhys. Lett. **3**, 945 (1987).
- [3] J. P. Renard, L. P. Regnault, and M. Verdaguer, J. de Phys. Coll. **49**, C8-1425 (1988).
- [4] K. Katsumata *et al.*, Phys. Rev. Lett. **63**, 86 (1989).
- [5] S. Ma *et al.*, Phys. Rev. Lett. **69**, 3571 (1992).
- [6] T. Takeuchi *et al.*, J. Phys. Soc. Jpn. **61**, 3262 (1992).
- [7] L. P. Regnault *et al.*, Phys. Rev. B **50**, 9174 (1994).
- [8] G. E. Granroth *et al.*, Physica B **211**, 208 (1995).
- [9] A. Zheludev *et al.*, Phys. Rev. B **53**, 15004 (1996).
- [10] G. E. Granroth *et al.*, Phys. Rev. Lett. **77**, 1616 (1996).
- [11] I. Affleck *et al.*, Phys. Rev. Lett. **59**, 799 (1987).
- [12] M. Hagiwara *et al.*, Phys. Rev. Lett. **65**, 3181 (1990).
- [13] S. H. Glarum *et al.*, Phys. Rev. Lett. **67**, 1614 (1991).
- [14] A. P. Ramirez, S.-W. Cheong, and M. L. Kaplan, Phys. Rev. Lett. **72**, 3108 (1994).
- [15] S. R. White, Phys. Rev. Lett. **69**, 2863 (1992); Phys. Rev. B **48**, 10345 (1993).
- [16] S. Yamamoto and S. Miyashita, Phys. Rev. B **50**, 6277 (1994).

- [17] L. A. Desmaris *et al.*, Bull. Am. Phys. Soc. **40**, 327 (1995).
- [18] C. D. Batista, K. Hallberg, and A. A. Aligia, Phys. Rev. Lett. (pending).
- [19] H. Kikuchi *et al.*, J. Phys. Soc. Jpn. **64**, 3429 (1995).
- [20] H. Deguchi *et al.*, J. Phys. Soc. Jpn. **64**, 22 (1995).
- [21] Y. Ajiro *et al.*, J. Phys. Soc. Jpn. **66**, 2610 (1997).
- [22] P. P. Mitra, B. I. Halperin, and I. Affleck, Phys. Rev. B **45**, 5299 (1992).
- [23] M. Hagiwara, K. Katsumata, and T. Yosida, Hyper. Inter. **78**, 415 (1993).
- [24] M. Ito *et al.*, J. Phys. Soc. Jpn. **65**, 2610 (1996).
- [25] N. Fujiwara *et al.*, J. Magn. Magn. Mater. **140-144**, 1663 (1995).
- [26] V. Gadet *et al.*, unpublished.
- [27] L.-K. Chou *et al.*, Physica B **194-196**, 313 (1994). At the end of this paper, an error was made in estimating the length of the chains, and the corrected values are approximately 1,600 spins or about 0.9  $\mu\text{m}$ .
- [28] L.-K. Chou, Ph. D. Thesis, University of Florida, 1996.
- [29] G. E. Granroth, Ph. D. Thesis, University of Florida, 1998.
- [30] We cannot completely eliminate the possibility that the temperature independent FWHM value is a consequence of dipole-dipole broadening.

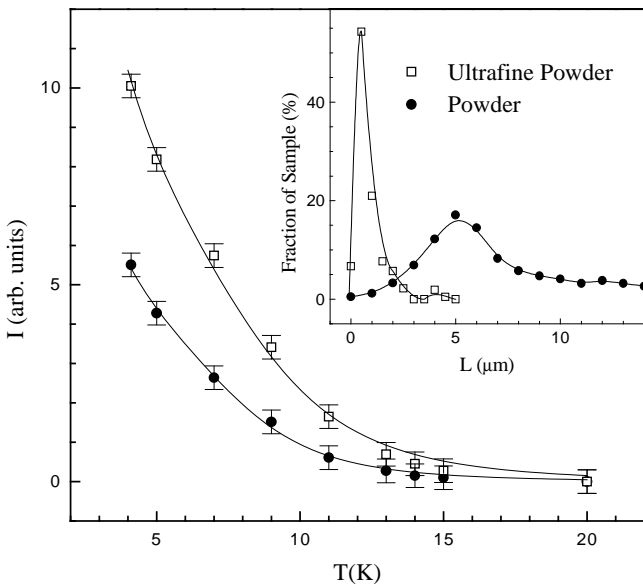


FIG. 1. Intensity of the 9.25 GHz ESR line for powder and ultrafine powder samples as a function of temperature. The solid lines are fits using Eq. (2), as described in the text. The inset shows typical percentage distributions of particle sizes for powder and ultrafine powder samples. The lines are included as guides to the eye.

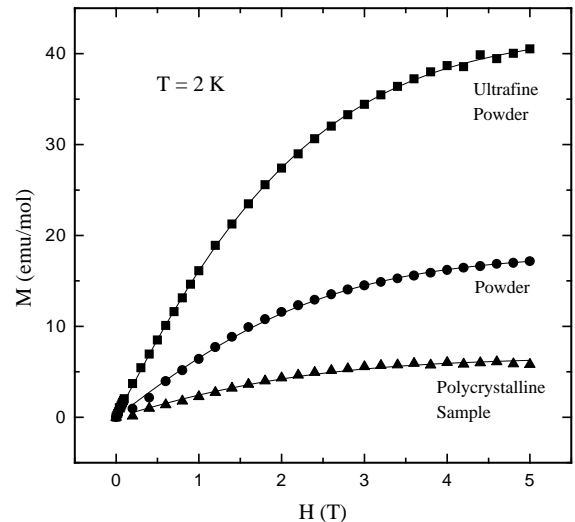


FIG. 2.  $M(H, 2\text{ K})$  for polycrystalline, powder, and ultrafine powder samples. The experimental uncertainties are given by the size of the data points. The solid lines represent fits to the sum of two Brillouin functions, Eq. (1), as described in the text.

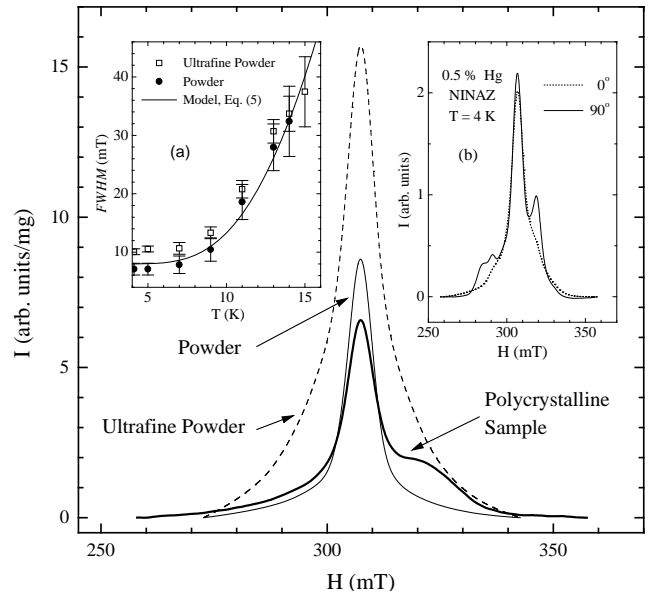


FIG. 3. Typical 9.25 GHz ESR line shapes for polycrystalline, powder, and ultrafine powder samples. Inset (a) shows the temperature dependence of the FWHM. The solid line represents a fit using Eq. (5), as described in the text. Inset (b) shows the orientational dependence of a 0.5% Hg doped sample, and this behavior is absent in the undoped polycrystalline specimen.

	Polycrystalline Sample	Powder	Ultrafine powder
$N_{1/2}$	$1000 \pm 60$	$2840 \pm 50$	$6280 \pm 50$
$N_1$	$20 \pm 10$	$30 \pm 9$	$140 \pm 8$

TABLE I.  $N_{1/2}$  and  $N_1$  (in ppm) of  $S = \frac{1}{2}$  and  $S = 1$  spins in the polycrystalline, powder, and ultrafine powder samples as deduced by fitting the  $M(H, 2\text{ K})$  data (Fig. 2) to Eq. (1).